

Realization of quantum Maxwell's demon with solid-state spins

W.-B. Wang¹, X.-Y. Chang¹, F. Wang¹, P.-Y. Hou¹, Y.-Y. Huang¹, W.-G. Zhang¹, X.-L. Ouyang¹, X.-Z. Huang¹, Z.-Y. Zhang², L. He¹, L.-M. Duan^{1,2}

¹*Center for Quantum Information, IIIS, Tsinghua University, Beijing 100084, PR China*

²*Department of Physics, University of Michigan, Ann Arbor, Michigan 48109, USA*

(Dated: November 29, 2017)

Resolution of the century-long paradox on Maxwell's demon reveals a deep connection between information theory and thermodynamics. Although initially introduced as a thought experiment, Maxwell's demon can now be implemented in several physical systems, leading to intriguing test of information-thermodynamic relations. Here, we report experimental realization of a quantum version of Maxwell's demon using solid state spins where the information acquiring and feedback operations by the demon are achieved through conditional quantum gates. A unique feature of this implementation is that the demon can start in a quantum superposition state or in an entangled state with an ancilla observer. Through quantum state tomography, we measure the entropy in the system, demon, and the ancilla, showing the influence of coherence and entanglement on the result. A quantum implementation of Maxwell's demon adds more controllability to this paradoxical thermal machine and may find applications in quantum thermodynamics involving microscopic systems.

PACS numbers:

INTRODUCTION

Maxwell's Demon is a gedanken experiment introduced a century ago by Maxwell that has a seeming contradiction with the second law of thermodynamics [1, 2]. Suppose a box full of gas particles is separated into left and right sides and connected through a small gate controlled by a microscopic being called the demon. When a gas particle comes towards the gate, the demon only opens the gate when it observes that the particle is from the left. Due to this selective opening of the gate, eventually all the gas particles move to the right side, and the system entropy thus decreases which seemingly contradicts with the second law of thermodynamics. After decades of controversies in the interpretation, this paradox is finally resolved by the observation that the demon has to acquire information about the gas particle for each gate operation [1–5]. Erasing of this information transfers a finite amount of work to heat (Landauer's principle) and thus the demon's own entropy increases which is always no less than the entropy decrease in the system [1–8].

The essence of Maxwell's demon experiment is the information acquiring by the demon and the feedback to the system depending on this information. This thought experiment has been implemented in several physical systems, where the entropy decrease and the transferring of heat to work in the system has been observed [9–18]. The demon's operations could also be implemented by quantum gates using microscopic qubits [6–8]. A quantum implementation allows the investigation of the role of quantum coherence and entanglement in the microscopic limit of thermal machines, a topic that raised significant interest in the rising field of quantum thermodynamics [19–22]. In particular, entanglement could be interpreted as a resource of negative entropy for some thermodynamic process [21]. Very recently, Maxwell's demon has been demonstrated using the nuclear magnetic resonance and the superconducting cavity systems based on quantum gate operations [23, 24]. In those experiments, the demon still starts at a classical state and the role of entanglement has not been investigated yet.

Here, we report an experimental realization of quantum Maxwell's demon based on control of solid-state spins which demonstrates the important role of memory consumption and entanglement in the functionality of a quantum demon. A key observation to the resolution of Maxwell's demon paradox is that the operation by the demon consumes its memory and without a memory reset it will not be able to continuously reduce the system entropy. To demonstrate this key point, we use electronic spin states to represent the demon's memory and experimentally observe that the same demon's operation successively on two nearby nuclear spins reduces the entropy of the first system but fails to do so for the second one. Then, we prepare the demon in a quantum superposition state and demonstrate that the entropy decrease in the system depends on the observation basis. Finally, to demonstrate the important role of entanglement, we entangle the demon at the beginning with an ancilla representing an insider observer. For an outside observer without access to the ancilla's information, the demon's operation fails to reduce the system entropy. However, for an inside observer with help from the ancilla, we show that the entropy for both the system and the demon can decrease while the ancilla's entropy remains the same. This contradiction with the interpretation of the classical demon therefore experimentally confirms that the entanglement can serve as a resource of negative entropy

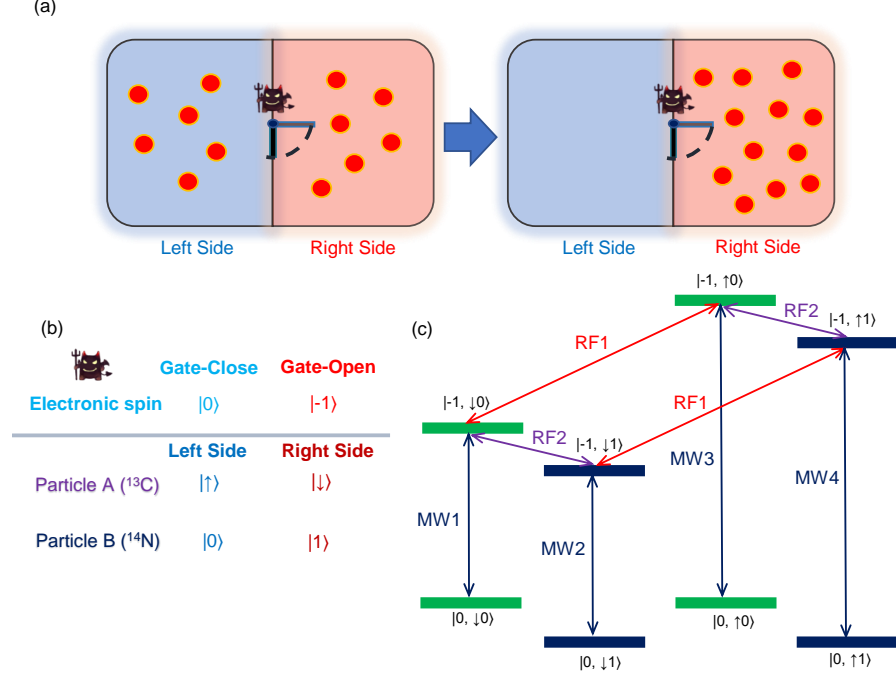


FIG. 1: **Implementation of quantum Maxwell's demon with solid state spins.** **a**, Illustration of the Maxwell's demon paradox. A box with gas particles is separated into two sides. A demon at the middle detects which side the particle comes from (information acquiring) and only opens the gate if the particle is from the left side (feedback). Eventually all the particles move to the right side and the system entropy decreases which seemingly contradicts with the second law of thermodynamics. **b**, Implementation of Maxwell's demon with three solid-state quantum spins. The demon's memory is represented by the electronic spin state, which controls opening or closing of the gate. Two particles A and B are represented by nuclear spins ^{13}C and ^{14}N , where the left or right sides of the particles are encoded with two orthogonal spin states. The information acquiring and feedback operations by the demon are implemented through conditional quantum gates. **c**, The hyperfine level structure of the electronic and the nuclear spins. The hyperfine interactions and the applied external magnetic field split all the energy levels and differentiate their transition frequencies. Based on the frequency selection, the applied microwave or RF fields selectively drive a certain set of transitions and make the conditional quantum gates.

for the quantum Maxwell's demon [21].

RESULTS

Implementation of quantum Maxwell's demon with solid state spins

To implement quantum Maxwell's demon, we use electronic spin and nuclear spins in a nitrogen vacancy (NV) center of a room-temperature diamond sample to carry the states of the system and the demon. The spins in diamond NV centers provide a promising solid-state system for realization of quantum information processing and nanoscale sensing, which has attracted a lot of interest in recent years [25–34]. The ground state of the NV center has electronic spin $S = 1$, which interacts with the dopant ^{14}N with nuclear spin $I = 1$ and the nearby ^{13}C isotopes with nuclear spin $I = 1/2$ in the host diamond through hyperfine coupling, forming a small quantum spin register [25, 26]. As shown in Fig. 1a and 1b, in our experiment we use the $|0\rangle$ and $|-1\rangle$ states of the NV electronic spin to represent the demon's status for gate closing and opening, respectively. In the first experiment, we use the states of $|\uparrow\rangle$ and $|\downarrow\rangle$ of a ^{13}C nuclear spin with the hyperfine splitting of 6.5 MHz to represent the location of the first particle (particle A) in the left or right side of the box. To test successive operation of the demon, we introduce the second particle (particle B), whose location is represented by the $|0\rangle$ and $|1\rangle$ states of the ^{14}N nuclear spin with the energy

splitting about 2.8 MHz. The relevant level structure of the electronic and the nuclear spins in the NV center is Fig. 1c, and the transitions between these levels can be manipulated through application of microwave or radio frequency (RF) pulses at the corresponding frequencies.

The operation of Maxwell's demon has two components. The first component is information acquiring which changes its memory state depending on the side of incoming particle and in our case is realized through the quantum controlled-NOT gate $C_C\text{-NOT}_E$ or $C_N\text{-NOT}_E$, where the electronic spin state representing the demon's memory flips conditional on the control particle (^{13}C or ^{14}N nuclear spin). The second component is a feedback operation where the demon opens the gate conditional on its memory in the $|1\rangle$ state and the incoming particle changes its side in the box. In our case, this feedback operation is realized through the conditional quantum gate $C_E\text{-NOT}_C$ or $C_E\text{-NOT}_N$ for the first and the second particles, respectively. The quantum circuit that implements the Maxwell's demon operations is shown in Fig. 2a.

For Maxwell's demon experiment, the system starts at a mixed state where the particles have equal probabilities to be in the left or right side of the box while the demon's memory is at a pure state so that it can track the particle's information. In our experiment, we apply a weak external magnetic field of 38 Gauss to split the energy levels $|1\rangle$ and $|-1\rangle$ of the electronic spin, and the field is small enough so that the nuclear spins remain at the completely mixed states when we polarize the electronic spin to the $|0\rangle$ state through optical pumping. The CNOT gates for the demon's information acquiring operation are implemented through two microwave pulses and for the demon's feedback operation are implemented through a RF pulse. For instance, with the level structure shown in Fig. 1c, application of π -pulses with MW3 and MW4 (MW2 and MW4) realize the $C_C\text{-NOT}_E$ ($C_N\text{-NOT}_E$) gate, and application of π -pulses with RF1 (RF2) realize the $C_E\text{-NOT}_C$ ($C_E\text{-NOT}_N$) gate. The typical experimental sequence is shown in Fig. 2b.

The essence of Maxwell's demon is to reduce the entropy of the system at the cost of entropy increase of its own memory. To characterize the entropy flow for the system and the demon, we directly measure the entropy of the system and the demon through quantum state tomography before and after the demon's operation on the first and the second particles. Quantum state tomography is implemented with a set of microwave and RF pulses that rotate the detection basis and then optical read-out of the electronic spin state by detection of fluorescence (see the Methods). For outcome states i measured to occur with probability p_i , the entropy is defined as $S = -\sum_i p_i \log_2 p_i$, where the base is taken to be 2 for convenience. For comparison between the experimental state (constructed as a density matrix ρ_e) and the outcome state ρ_{id} in the ideal case, we also measure the state fidelity F , which is defined as $F = [\text{tr}(\sqrt{\sqrt{\rho_{\text{id}}}\rho_e\sqrt{\rho_{\text{id}}}})]^2$.

The measurement results for the state fidelity F and the entropy S are shown in Fig. 2c and 2d. Before the demon's operation, both particles (nuclear spins) are in the maximally mixed states with entropy $S = 1$. The demon (electronic spin) is in a pure state with a high fidelity (our calibration of the fluorescence levels for detection has subtracted the initialization imperfection by the green laser, see the Methods), but its entropy is measured to be $0.10^{+0.10}_{-0.09}$ as the value of S is extremely sensitive to small imperfection near a pure state by its definition. In the supplementary information, we provide an analysis of noise and plot the entropy as a function of the system noise and the purity of quantum state. From the plot, one can immediately see the sensitivity of entropy under small drop of the purity of quantum state. After the demon's operation on the first particle, the system (particles A and B) entropy decreases as expected while the entropy for the demon's memory increases. Due to the sensitivity of S to small imperfection, the measured value of S for particle A is $0.36^{+0.04}_{-0.05}$ although it has a high fidelity of $95.5^{+0.8}_{-0.8}\%$ to a pure state, where the numbers in the superscript and the subscript denote a confidence interval with probability of 68%. We then continue to apply the demon's operation on the second particle. As the demon has run out of its memory (which is only 1 bit in this experiment), the successive operation of the demon on the second particle does not cause any entropy decrease for the system as one can see from the measurement result in Fig. 2d. This confirms that the consumption of information storage capacity in the demon's memory is essential for its operation, a key concept for the resolution of Maxwell's demon paradox with the second law of thermodynamics.

From the above data, one can see that the entropy decrease in the system is always bounded by the information acquired by the demon during the readout step, a key observation in interpretation of the Maxwell's demon experiment. For instance, for the demon's interaction with particle A, the entropy decrease in the system is 0.58. while the information acquired by the demon is given by 0.81. For the demon's interaction with particle B, although the operations are the same, as the demon runs out of its memory, the information acquired by the demon is diminishing. So this limits the entropy decrease of the particle B by the demon's operation, measured to be 0 within the experimental uncertainty from Fig. 2.

In our experiment, the measurements are focused on detection of the entropy flow for two reasons: first, the entropy plays a critical role for interpretation of the Maxwell's demon paradox and its resolution with the second law of

thermodynamics. Second, in our system it is more convenient to measure the entropy flow, which is complementary to the demonstration of classical Maxwell's demon in other systems where it is typically easier to measure the energy extraction instead of the entropy flow [9–13]. Although we cannot directly measure the work extraction in this experimental system, the entropy decrease is closely related to the amount of work that can be extracted from the system as discussed in Ref. [6]. In principle, the work could be extracted through stimulated emission by shining a microwave pulse resonant to this spin although in practice it is hard to realize that experimentally on a single spin. The measured entropy decrease provides an upper bound on the amount of work that could be extracted from the system through the Landauer's principle [2–7].

Maxwell's demon in a quantum superposition state

Next we prepare Maxwell's demon (the electronic spin in our case) initially at a quantum superposition state $(|0\rangle + |1\rangle)/\sqrt{2}$ and test influence of quantum coherence to the demon's operation. For this experiment, we use the ^{13}C nuclear spin as our system particle, which initially needs to be in a mixed state. However, it is better to polarize the ^{14}N nuclear spin otherwise it works as a decoherence source for the electronic spin when the latter is in a superposition state. We therefore tune the external magnetic field to a value of 340 Gauss, and under this value of magnetic field, the ^{14}N nuclear spin has a strong enough spin-exchange interaction with the electronic spin at the excited state so that it gets polarized by the optical pumping, while the ^{13}C nuclear spin only undergoes a weak spin-exchange interaction and remains to be mixed. The demon's operation is achieved by the same set of quantum gates. The only difference is that we need to apply dynamical decoupling pulses, which induce a fast π rotation along the X or Y spin axis, to the electronic spin before and after the long RF pulse for the $\text{C}_\text{E}\text{-NOT}_\text{C}$ gate to remove the coupling of the electronic spin to the spin bath and keep its coherence. The experimental pulse sequence is shown in Fig. 3a. After the demon's operation, if we measure the system in the classical basis (the computational basis $|\uparrow\rangle$ and $|\downarrow\rangle$), the system entropy does not show any decrease. This can be easily understood as a demon in an equal quantum superposition of classical states is just like a maximally mixed state looking from a measurement in the classical basis. However, if we measure the system in the superposition basis, the system entropy does decrease. The state fidelity and the measured entropy under different bases are shown in Fig. 3b and 3c. So when the demon hides its information storage capacity in the quantum superposition state, maintaining coherence is important for functioning of the quantum demon.

Maxwell's demon in an entangled state with an ancilla

Entanglement represents the key feature of a quantum system, and it provides new possibilities for a quantum Maxwell's demon. When we prepare the demon in a maximally quantum entangled state with an ancilla, to an outside observer who has no access to information in the ancilla, the demon appears to be in a maximally mixed state and thus it has no information storage capacity to reduce the system entropy by the demon's operation. However, an inside observer who has access to the ancilla can make use of this entanglement and find that the entropy in both the system and the demon can decrease with feedback from the ancilla. This provides a nice demonstration that entanglement can serve as a source of negative entropy for a quantum thermal machine [21].

To demonstrate Maxwell's demon starting from an entangled state, we still tune the external magnetic field to 340 Gauss and polarize both the electronic spin (the demon) and the ^{14}N nuclear spin (the ancilla) by the optical pumping, which leaves the ^{13}C nuclear spin (the system) in an almost maximally mixed state. Then, we can apply the microwave and RF pulses as shown in Fig. 4a to prepare the demon and the ancilla in a maximally entangled state $|\Phi_\text{DA}\rangle = (|0, 0\rangle - |-1, 1\rangle)/\sqrt{2}$. The RF pulse for the gate $\text{C}_\text{E}\text{-NOT}_\text{N}$ is long, so the electronic spin coherence needs to be protected by the dynamical decoupling pulses. Furthermore, this RF pulse also induces a phase shift for the electronic spin by off-resonant coupling, which is calibrated and compensated by the phase of subsequent microwave pulses applied on the electronic spin. After the state preparation, we have measured the entanglement between the demon and the ancilla, with the result shown in Fig. 4b. From the reconstructed density matrix ρ_DA of the demon and the ancilla from quantum state tomography, we find that the entanglement fidelity, defined as $F_\text{e} = \langle \Phi_\text{DA} | \rho_\text{DA} | \Phi_\text{DA} \rangle$, is $91.0^{+1.3}_{-1.5}\%$ for this initial state, which confirms entanglement.

The demon's operation is achieved by the same set of gates as shown in Fig. 4a. The coherence of the electronic spin during the conditional gate $\text{C}_\text{C}\text{-NOT}_\text{E}$ needs to be protected by the dynamical decoupling pulses, whose spin rotation axis is chosen to be the same as that of the microwave pulses for the $\text{C}_\text{C}\text{-NOT}_\text{E}$ gate, therefore the dynamical decoupling commutes with and does not affect the gate operation. After the demon's operation, we immediately perform measurements on the system and demon, emulating the measurement capability of an outside observer who

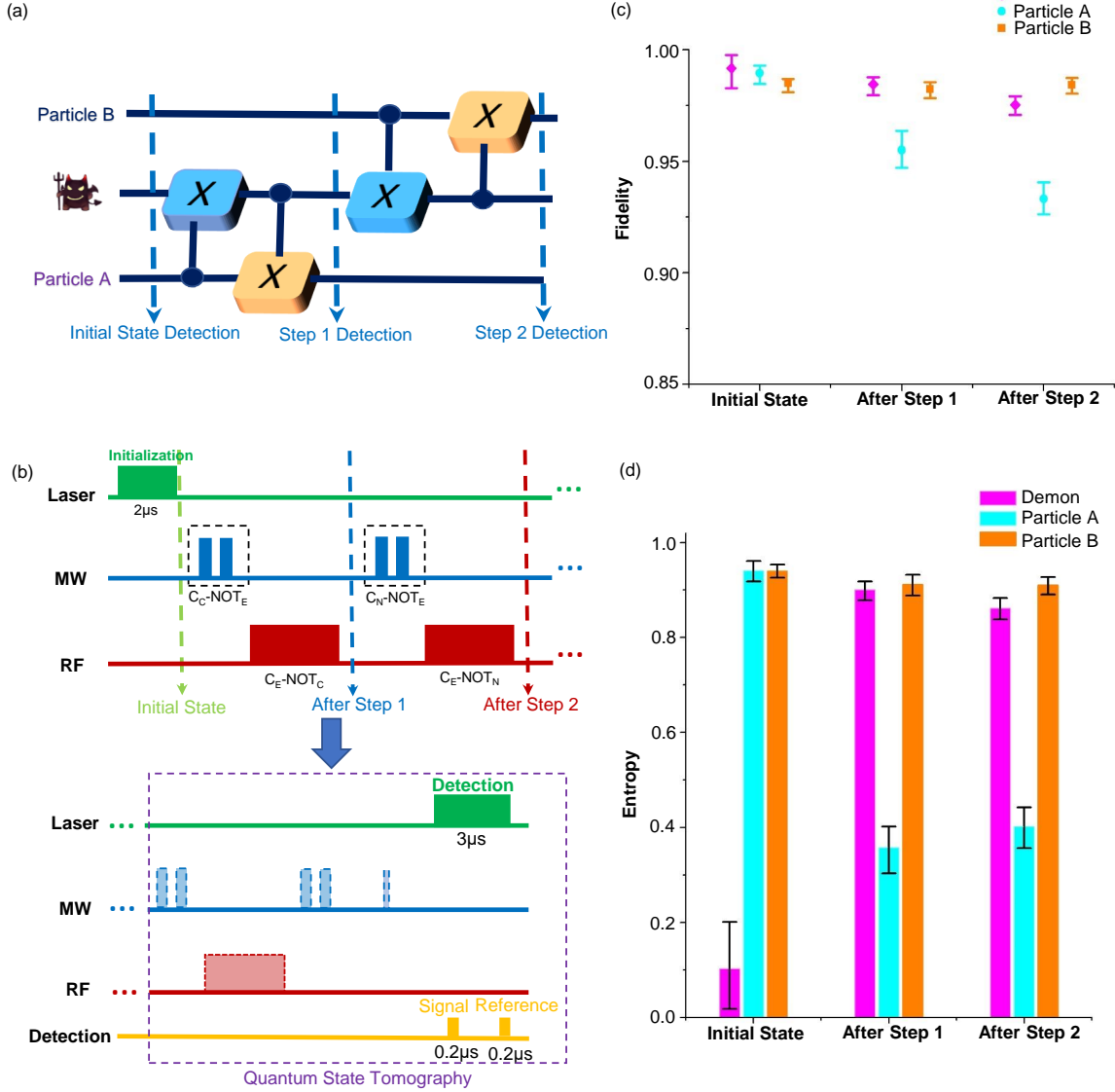


FIG. 2: **Maxwell's demon under successive operations.** **a**, The quantum circuit represents the demon's operations successively on the first (A) and the second (B) particles. Each demon's operation consists of two controlled-NOT quantum gates respectively for information acquiring and feedback. We detect the state of the demon, particle A, and particle B at the beginning and after the first (step 1) and the second (step 2) demon's operation. **b**, Experimental sequence of laser, microwave, and RF pulses for implementation of the successive demon's operations on particles A and B. Each conditional gate on the electronic spin is implemented by two microwave pulses on the corresponding transitions. The conditional gates on the nuclear spins are realized through RF pulses. The detections at the beginning, step 1, and step 2 are done through quantum state tomography, which consists of several microwave and RF pulses to rotate the measurement bases followed by the optical readout of the electronic spin state (see the Methods). **c**, The measured state fidelity of the demon and particles A and B at the beginning and after step 1 and step 2 compared with the ideal states at the corresponding stages. **d**, The entropy of the system and particles A and B measured through quantum state tomography at the three corresponding stages. The error bars in all the figures denote the confidence interval with probability of 68%, which corresponds to one standard deviation if the underlying distribution is Gaussian.

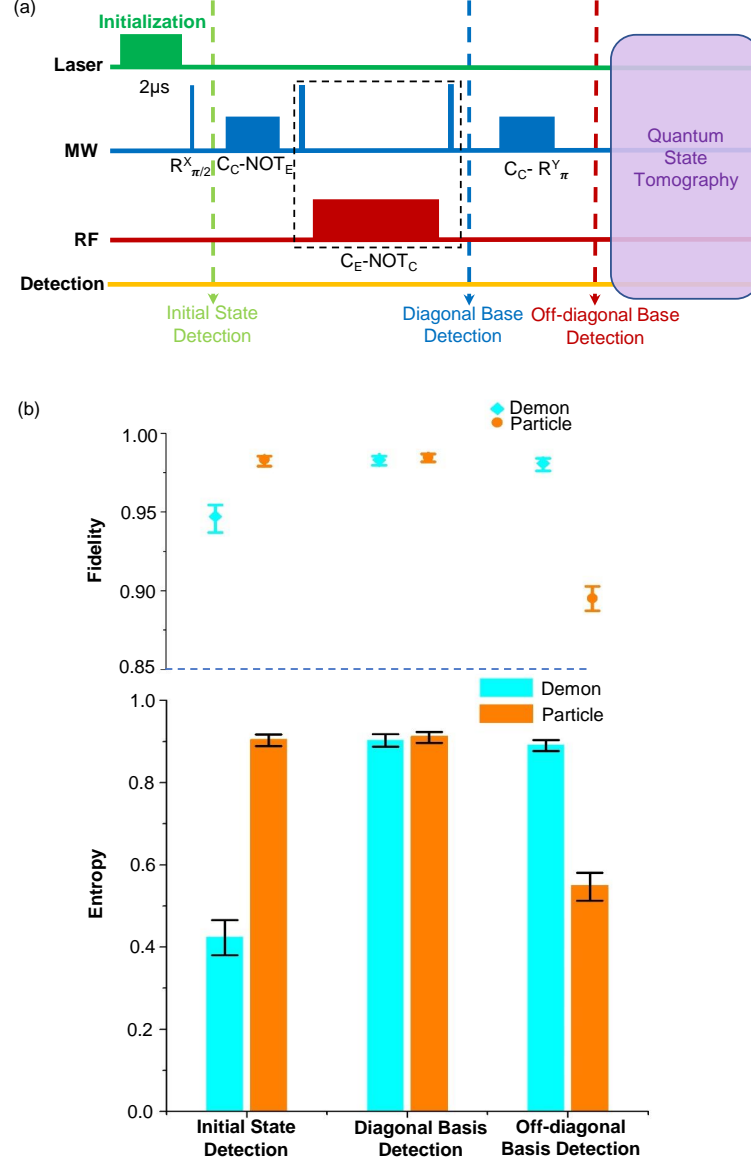


FIG. 3: **Maxwell's demon in a quantum superposition state.** **a**, The experimental sequence of laser, microwave, and RF pulses. The first microwave pulse $R_{\pi/2}^X$ induces a $\pi/2$ rotation along the X spin-axis and prepares the demon in an equal superposition state. The demon's operation between the electronic spin and the ^{13}C nuclear spin is achieved through the same conditional quantum gates, with the only difference of addition of two dynamical decoupling π -pulses to remove the dephasing noise of the electronic spin during the slow RF pulse on the nuclear spin. We detect the output state in both the diagonal (computational) and off-diagonal bases. For detection in the off-diagonal basis, we first apply a conditional gate (a microwave pulse $C_C - R_{\pi}^Y$) to disentangle the electronic and the nuclear spins as the demon's operation entangles them when the demon starts in a superposition state. **b**, The measured state fidelity and entropy at the beginning and after the demon's operation. The final state is detected in both the diagonal and the off-diagonal bases. The fidelity denotes the comparison between the experimental states and the ideal states at the corresponding stages.

does not have access to the ancilla. In this case, with the result shown in Fig. 4c, we find that the entropy of both the system and the demon are at the maximum level and do not show any decrease by the demon's operation. This is expected as without access to the ancilla, the demon's entanglement information cannot be retrieved and it has no memory capacity to reduce the system entropy.

We then emulate the capability of an inside observer and perform the feedback operation between the demon and the ancilla shown in Fig. 4a. Same as the demon operation, this is done by applying the gates $C_E - \text{NOT}_N$ and $C_N - \text{NOT}_E$

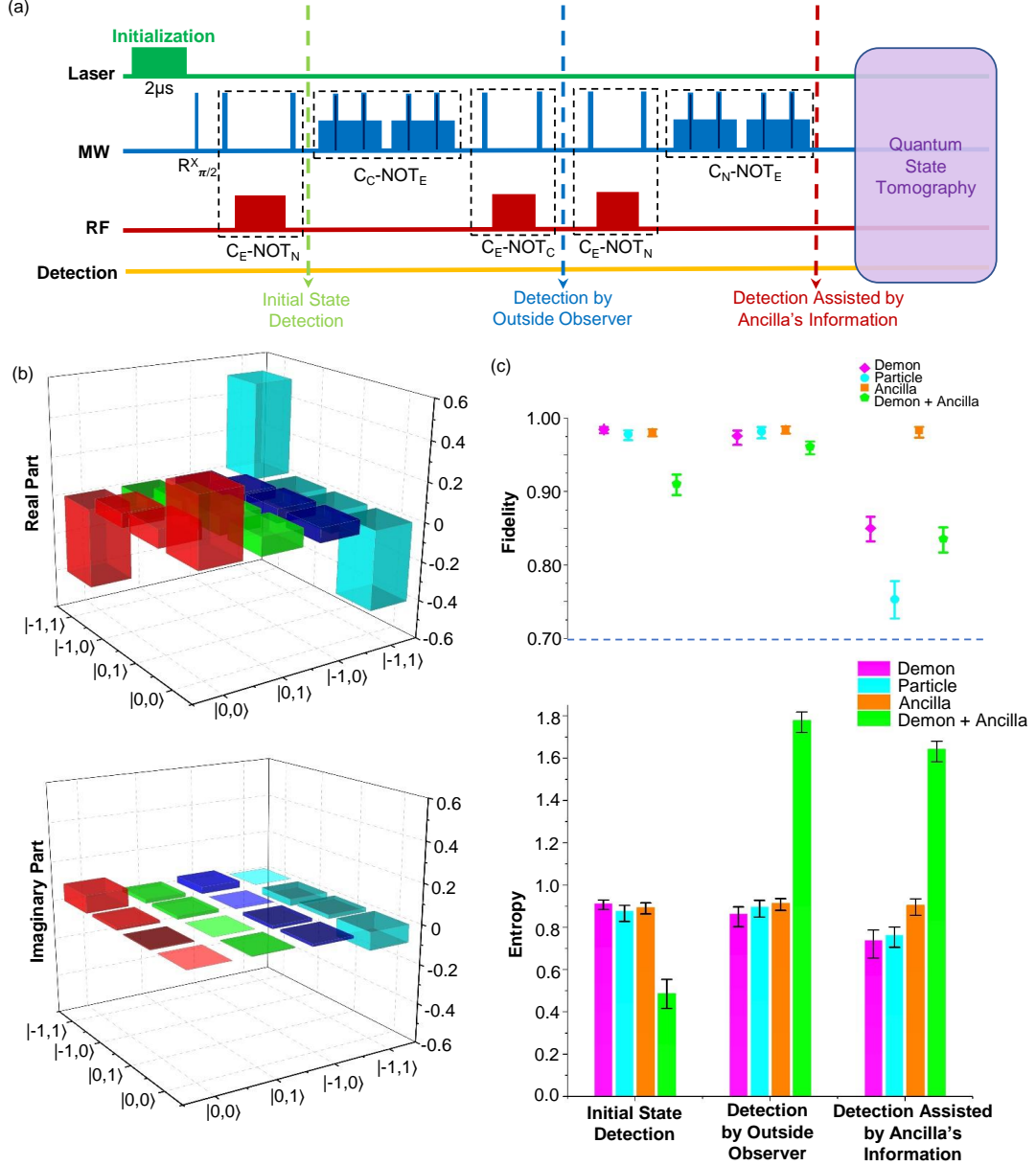


FIG. 4: **Maxwell's demon in an entangled state with an ancilla.** **a**, The experimental Pulse sequence for initial entangled state preparation, the demon's operation, and final state detection under different scenarios. The first part prepares a maximally entangled state $(|0,0\rangle - |1,1\rangle)/\sqrt{2}$ between the demon (the electronic spin) and the ancilla (the ^{14}N nuclear spin). The demon's operation is the same as those in Fig. 3, with the difference that now the microwave pulse becomes slow as one needs to resolve the level splitting of the ^{14}N nuclear spin and the electronic spin coherence during the slow microwave pulse is protected by dynamical decoupling as well. For the final state detection, an outside observer detects directly the demon (the electronic spin) and the system (the ^{13}C nuclear spin), while an inside observer, with access to the ancilla's information, applies two coherence-protected conditional quantum gates between the electronic spin and the ^{14}N nuclear spin before quantum state tomography on the system and the demon, and obtains results inaccessible to the outside observer and incompatible with interpretation of classical Maxwell's demons. The system and the demon are disentangled by a microwave pulse (corresponding to a $C_C - NOT_E$ gate) in quantum state tomography. **b**, Real and imaginary parts of the reconstructed density matrix elements for the initial entangled state between the demon and the ancilla. **c**, The measured state fidelity and entropy at the beginning and after the demon's operation. The results for the final state are shown for both the outside and the inside observers with and without access to the ancilla's information, respectively. The notation "Demon + Ancilla" corresponds to a detection of the joint state and the von Neumann entropy for this composite system, while the others correspond to detection of each individual system.

(with coherence protected by the dynamical coupling). After the gates, we perform quantum state tomography on the system and the demon (they are disentangled by a gate $C_C\text{-NOT}_E$), and the resultant entropy is shown in Fig. 4c. For this inside observer, the entropies for the system and for the demon both decrease. In the ideal case, the entropy should decrease to zero, however, in experiments because of sensitivity of the value of entropy to imperfections near a pure state, we find the entropy only decreases a bit although the fidelity to a pure state is given by $85.0^{+1.6}_{-1.8}\%$ and $75.3^{+2.5}_{-2.6}\%$ for the demon and the system, respectively. As the ancilla's entropy remains almost the same before and after the demon's operation, if we add up the total entropy of the system, the demon, and the ancilla, they decrease by the demon's operation. This is impossible for a classical demon, however, in the quantum case, with feedback from the ancilla, we use one bit of entanglement, which can convert to two bits of negative entropy [21], and therefore it is possible to reduce the entropy for both the system and the demon. When there is entanglement, we need to count entropy by a collective measurement on the demon and the ancilla in an entangled basis instead of adding up their individual entropies, and as shown in Fig. 4, the total entropy counted in this way then increases and there is no inconsistency with the second law of thermodynamics by taking into account of the contribution of entanglement.

DISCUSSION

We have implemented the Maxwell's demon experiment using a quantum system with three solid-state spins in a diamond sample. Our experiment demonstrates for the first time the role of quantum entanglement in the Maxwell's demon. We have prepared the demon in a quantum entangled state with an ancilla and demonstrated that the entanglement provides a resource of negative entropy for the system and the demon if the observer has access to the ancilla's information [21]. Through successive application of the demon's operation on system particles, we have also demonstrated that the memory capacity of Maxwell's demon is critical for its functioning, an observation important for the resolution of this paradox with the second law of thermodynamics [2–6].

A quantum implementation of Maxwell's demon, in particular with access to the entangled states, deepens our understanding of the interplay between thermodynamics and quantum entanglement and sheds new light on the profound connection between the fundamental principles of thermodynamics and quantum information theory [6–8, 19–22]. The quantum control techniques in the Maxwell's demon experiment may also find applications in implementation of other quantum thermal machines involving microscopic systems [19–22].

METHODS

Experimental setup

We use a home-built confocal microscopy with an oil immersed objective lens to address and detect single nitrogen vacancy (NV) centers in a single-crystal diamond sample, which is mounted on a doughnut shape, three-axis, closed-loop piezoelectric actuator with sub-micron resolution. A 532 nm diode laser, controlled by an acoustic optical modulator (AOM), is used for spin state initialization and detection. Fluorescence photons (wavelength ranging from 637 to 850 nm) are collected into a single-mode fibre and detected by a single photon counting module (SPCM). To deliver the microwave signal to the NV center, we use a gold coplanar waveguide (CPW), which has a small Ω -shape structure (of 60 μm length) near the NV to enhance the coupling. To deliver the RF signals to the NV center, we set a gold coil above the sample. The coil has 0.5 cm diameter and 50 turns, with 20 μm gaps between the gold lines.

We scan the sample and find a single NV center coupled with a proximal ^{13}C nuclear spin of 6.5 MHz hyperfine coupling strength for our experiment. The external magnetic field is applied through a permanent magnet, which is tuned to 38 G along the NV axis for the first experiment and to 340 G for the second and third experiments. We use an arbitrary-waveform generator (AWG, Tektronix with 1 GHz sampling rate) to control the time sequence of our experiment. The digital markers of the AWG are used to control the pulse sequence with a timing resolution of 1 ns. The RF signals for control of nuclear spins and the digital signals for switch of the photon counters and the home-built field programmable gate array (FPGA) circuit are directly generated from the AWG. The microwave signals from a generator (MXG Analog Signal Generator, Keysight with 9kHz-6GHz frequency) are mixed with the control signals from the AWG via IQ mixers. All the microwave and RF signals are amplified by independent amplifiers.

For each experimental cycle, We collect signal photons for 200 ns right after the detection laser rises and reaches the full intensity, and for another 200 ns for reference 2 μs later. We repeat the experimental cycle at least 4×10^6 times, resulting in a total photon count over 5×10^4 . The error bars of our data describe the statistical error which comes from the photon counting. To calculate the error bar for each experimental quantity, we use Monte Carlo sampling by

assuming a Poissonian distribution for the photon counts and propagate the statistical distribution from the measured data to the calculated quantity through exact numerical simulation. This simulation based on Monte Carlo sampling gives the statistical distribution for the target quantity, from which we can easily calculate the confidence intervals. The error bars in the paper denote an confidence interval with probability of 68.3%, which corresponds to one standard deviation if the underlying distribution is Gaussian.

Experimental calibration and quantum state tomography

The fluorescence levels of electronic spin $|0\rangle$ and $|-1\rangle$ states, as well as the contrast between them, vary slightly for different experimental cycles due to temperature variation or change of the laser power. To cancel out the influence of this variation, before each measurement sequence we calibrate the fluorescence levels of the electronic spins in $|0\rangle$ and $|-1\rangle$ states and use this as the standard to normalize our experimental data in the measurement sequence. For this calibration, we have neglected the imperfection of microwave π -pulse to flip between the electronic spin $|0\rangle$ and $|-1\rangle$ states. By this calibration, we have subtracted the state initialization and detection errors in the computational basis. The state infidelities reported in the paper comes from the accumulated errors of a sequence of quantum gates used for the demon operations and quantum entanglement as well as the decoherence contribution during this sequence of quantum gates.

We use quantum state tomography to measure the density matrix of the final state. The electronic spin state is directly measured by its corresponding fluorescence levels together with microwave pulses to rotate the measurement basis. The nuclear spin states for ^{13}C or ^{14}N are first mapped to the electronic spin states with a microwave pulse at the appropriate frequency for measurement of their fluorescence levels, with the calibration procedure same as those described in the method section of Ref. [33]. For the ^{14}N nuclear spin, we only use its $|0\rangle$ and $|1\rangle$ states to represent the qubit, and its population in the $|-1\rangle$ level, when exists, only contributes to the background contrast in calibration of the fluorescence. The rotation of the nuclear spin measurement basis is achieved through a RF pulse at the corresponding frequency.

State transformation in the third experiment

Here, we work out the step-by-step state transformation for the third experiment where the demon (the electronic spin) starts in an entangled state of the form $|\Psi_0\rangle_{\text{EN}} = (|0\rangle_{\text{E}}|0\rangle_{\text{N}} - |-1\rangle_{\text{E}}|1\rangle_{\text{N}})/\sqrt{2}$ with the ancilla (the nitrogen nuclear spin). Note that the reduced initial state of the demon is given by a fully mixed 2×2 identity matrix I_{E} . The system (the C^{13} nuclear spin) is initially prepared in a full mixed state described by the identity matrix I_{C} (this C^{13} nuclear spin will not be polarized by optical pumping under the 340 G magnetic field as verified in the experiment). After the demon's operation $\text{C}_{\text{E}}\text{-NOT}_{\text{C}}\text{C}_{\text{C}}\text{-NOT}_{\text{E}}$, the state transforms to $\rho_{\text{ECN}} = (|\Phi_1\rangle\langle\Phi_1| + |\Phi_2\rangle\langle\Phi_2|)/2$, where $|\Phi_1\rangle = (|0\rangle_{\text{E}}|\uparrow\rangle_{\text{C}}|0\rangle_{\text{N}} + i|-1\rangle_{\text{E}}|\downarrow\rangle_{\text{C}}|1\rangle_{\text{N}})/\sqrt{2}$ and $|\Phi_2\rangle = (|0\rangle_{\text{E}}|\downarrow\rangle_{\text{C}}|1\rangle_{\text{N}} + i|-1\rangle_{\text{E}}|\uparrow\rangle_{\text{C}}|0\rangle_{\text{N}})/\sqrt{2}$. For an outside observer who does not have access to the information of the ancilla, the system and demon's state is described by the reduced density matrix $I_{\text{C}} \otimes I_{\text{E}}$. This is a completely mixed state and the entropy in either the system or the demon does not show any decrease, as confirmed by the experimental observation. However, for an inside observer who has access to the ancilla, the observer can apply joint operations $\text{C}_{\text{N}}\text{-NOT}_{\text{E}}\text{C}_{\text{E}}\text{-NOT}_{\text{N}}$ on the ancilla and the demon, which transforms the state to the form $[(|0\rangle_{\text{E}}|\uparrow\rangle_{\text{C}} + |1\rangle_{\text{E}}|\downarrow\rangle_{\text{C}})/\sqrt{2}] \otimes I_{\text{N}}$. The reduced state for the system and the demon becomes $(|0\rangle_{\text{E}}|\uparrow\rangle_{\text{C}} + |1\rangle_{\text{E}}|\downarrow\rangle_{\text{C}})/\sqrt{2}$. After another disentangling operation $\text{C}_{\text{C}}\text{-NOT}_{\text{E}}$, both the system and the demon are in the pure state $|-1\rangle_{\text{E}} \otimes (|\uparrow\rangle + |\downarrow\rangle)_{\text{C}}/\sqrt{2}$, and the entropy for either of them decreases by one bit in the ideal case. If we compare this case with the measurement by an outside observer (or with the initial state), we see that the entanglement with the ancilla effectively contributes two bits of negative entropies to the system and the demon with the ancilla assisted operations, reducing the entropy of each of them by one bit. This is similar in spirit to the scheme in Ref. [21]. For the experimental case, due to the sensitivity of entropy to imperfection near pure states and the sensitivity of entanglement to noise during a series of quantum operations, we observed an entropy decrease about 0.12 bit and 0.14 bit for the system and the demon, respectively. In the supplementary information, we take into account the contribution of dominant noise during the experiment, and the theoretical estimation agrees semi-quantitatively with the experimental observation. The observed entropy decrease, although significantly less than the amount predicted for the ideal case, still confirms the contribution of entanglement as a resource of negative entropy, as otherwise the total entropy for the system and the demon can only be increasing due to the second law of thermodynamics, in particular with the noise contribution during the experiment.

References

- [1] Maruyama, K., Nori, F. & Vedral, V. Colloquium: The physics of Maxwell's demon and information. *Rev. Mod. Phys.* 81, 1–23 (2009).
- [2] Landauer, R. & IBM, J. Res. Dev. 5, 183 (1961).
- [3] Bennett, C. The thermodynamics of computation—a review. *Int. J. Theor. Phys.* 21, 905–940 (1982).
- [4] Zurek, W. H. in *Frontiers of Nonequilibrium Statistical Physics Volume 135 of Nato Science Series B:* (eds. Moore, G. T. & Scully, M. O.) 151 (Plenum Press, 1984).
- [5] Zurek, W. H. Thermodynamic cost of computation, algorithmic complexity and the information metric. *Nature* 341, 119–124 (1989).
- [6] Lloyd, S. Quantum-mechanical Maxwell's demon. *Phys. Rev. A* 56, 3374–3382 (1997).
- [7] Vedral, V. Landauer's erasure, error correction and entanglement. *Proc. R. Soc. London, Ser. A* 456, 969. (2000).
- [8] Kim, S., Sagawa, T., De Liberato, S. & Ueda, M. Quantum Szilard Engine. *Phys. Rev. Lett.* 106, 70401 (2011).
- [9] Scully, M. O., Zubairy, M. S., Agarwal, G. S. & Walther, H. Extracting Work from a Single Heat Bath via Vanishing Quantum Coherence. *Science* 299, 862–864 (2003).
- [10] Serreli, V., Lee, C. F., Kay, E. R., and Leigh, D. A. Molecular Information Ratchet. *Nature*, 445. 523 - 527 (2007).
- [11] Raizen, M. G. Comprehensive Control of Atomic Motion. *Science* 324 (5933):1403–1406 (2009).
- [12] Toyabe, S., Sagawa, T., Ueda, M., Muneyuki, E. & Sano, M. Experimental demonstration of information-to-energy conversion and validation of the generalized Jarzynski equality. *Nat. Phys.* 6, 988 (2010).
- [13] Berut, A. et al. Experimental verification of Landauer's principle linking information and thermodynamics. *Nature* 483, 187–9 (2012).
- [14] Koski, J. V., Maisi, V. F., Sagawa, T. & Pekola, J. P. Experimental observation of the role of mutual information in the nonequilibrium dynamics of a Maxwell demon. *Phys. Rev. Lett.* 113, 30601 (2014).
- [15] Koski, J. V., Maisi, V. F., Pekola, J. P. & Averin, D. V. Experimental realization of a Szilard engine with a single electron. *PNAS* 111, 13786 (2014).
- [16] Koski, J. V., Kutvonen, A., Khaymovich, I.M., Ala-Nissila, T. & Pekola, J.P. On-Chip Maxwell's Demon as an Information-Powered Refrigerator. *Phys. Rev. Lett.* 115, 260602 (2015).
- [17] Vidrighin, M. D. et al. Photonic Maxwell's Demon. *Phys. Rev. Lett.* 116, 1-7 (2016).
- [18] Elouard, C., Herrera-Marti, D., Huard, B. & Auffeves, A. Extracting Work from Quantum Measurement in Maxwell's Demon Engines. *Phys. Rev. Lett.* 118, 260603 (2017).
- [19] Kieu, T. D. The second law, Maxwell's demon, and work derivable from quantum heat engines. *Phys. Rev. Lett.* 93, 140403 (2004).
- [20] Quan, H., Wang, Y., Liu, Y., Sun, C. & Nori, F. Maxwell's Demon Assisted Thermodynamic Cycle in Superconducting Quantum Circuits. *Phys. Rev. Lett.* 97, 180402 (2006).
- [21] Rio, L.D., Renner, R., Aaberg, J., Dahlsten, O. & Vedral, V. The thermodynamic meaning of negative entropy. *Nature* 474, 61 (2011).
- [22] Masanes, L. & Oppenheim, J. A general derivation and quantification of the third law of thermodynamics. *Nature Communications* 8, 14538 (2017).
- [23] Camati, P. A. et al. Experimental rectification of entropy production by a Maxwell's Demon in a quantum system. *Phys. Rev. Lett.* 117, 240502 (2016).
- [24] Cotteta, N., Jezouina, S., Bretheau, L., Campagne-Ibarcq, P., Flicheux, Q., Andersb, J., Auffeves, A., Azouitd, R., Rouchond, P. & Huard, B. Observing a quantum Maxwell demon at work. *Proc. Natl. Acad. Sci.* 114, 7561–7564 (2017).
- [25] Doherty, M. W. et al. The nitrogen-vacancy colour centre in diamond. *Physics Reports* 528, 1–45 (2013).
- [26] Childress, L., Walsworth, R. & M. Lukin. Atom-like crystal defects: From quantum computers to biological sensors. *Physics Today* 67, 38. (2014).
- [27] Jelezko, F. Gaebel, T., Popa, I. Gruber, A. & Wrachtrup, J. Observation of coherent oscillations in a single electron spin. *Phys. Rev. Lett.* 92. 076401 (2004).
- [28] Neumann, P., Mizuochi, N., Remp, F., Hemmer, P., Watanabe, H., Yamasaki, S., Jacques, V., Gaebel, T., Jelezko, F. & Wrachtrup, J. Multiparticle entanglement among single spins in diamond. *Science* 320, 1326 (2008).
- [29] Jacques, V., Neumann, P., Beck, J., Markham, M., Twitchen, D., Meijer, J., Kaiser, F., Balasubramanian, G., Jelezko, F. & Wrachtrup, J. Dynamic polarization of single nuclear spins by optical pumping of nitrogen-vacancy color centers in diamond at room temperature. *Phys. Rev. Lett.* 102. 057403 (2009).
- [30] Yao, N.Y., Jiang, L., Gorshkov, A.V., Maurer, P.C., Giedke, G., Cirac, J.I. & Lukin, M.D. Scalable architecture for a room temperature solid-state quantum information processor. *Nature Commun.* 3, 800 (2012).
- [31] Van Der Sar, T., Wang, Z. H., Blok, M. S., Bernien, H., Taminiau, T. H., Toyli, D. M., Lidar, D. A., Awschalom, D. D., Hanson R. & Dobrovitski, V. V. Decoherence-protected quantum gates for a hybrid solid-state spin register. *Nature* 484, 82 (2012).
- [32] Maurer, P. C., Kucsko, G., Latta, C., Jiang, L., Yao, N. Y., Bennett, S. D., Pastawski, F., Hunger, D., Chisholm, N., Markham, M., Twitchen, D. J., Cirac, J. I., Lukin, M. D.. Room-temperature quantum bit memory exceeding one second.

Science 336, 1283 (2012).

- [33] Zu, C., Wang, W.-B., He, L., Zhang, W.-G., Dai, C.-Y., Wang, F. & Duan, L.-M. Experimental realization of universal geometric quantum gates with solid-state spins. Nature 514, 72 (2014).
- [34] Pfaff, W. et al. Unconditional quantum teleportation between distant solid-state quantum bits. Science 10.1126, 1253512 (2014).

Acknowledgements This work was supported by the Ministry of Education and the National key Research and Development Program of China 2016YFA0301902. LMD and ZYZ acknowledges in addition support from the MURI and the ARL CDQI program.

Author Contributions L.M.D. designed the experiment and supervised the project. W.B.W, X.Y.C., F.W., P.Y.H., Y.Y.H., W.G.Z., X.L.O., X.Z.H., Z.Y.Z., L.H. performed the experiment. L.M.D. and W.B.W. wrote the manuscript.

Author Information The authors declare no competing financial interests. Correspondence and requests for materials should be addressed to L.M.D. (lmduan@umich.edu).

Supplementary information: Realization of quantum Maxwell's demon with solid-state spins

W.-B. Wang¹, X.-Y. Chang¹, F. Wang¹, P.-Y. Hou¹, Y.-Y. Huang¹, W.-G. Zhang¹, X.-L. Ouyang¹, X.-Z. Huang¹, Z.-Y. Zhang², L. He¹, L.-M. Duan^{1,2}

¹*Center for Quantum Information, IIIS, Tsinghua University, Beijing 100084, PR China*

²*Department of Physics, University of Michigan, Ann Arbor, Michigan 48109, USA*

PACS numbers:

SUPPLEMENTARY NOTE 1: ANALYSIS OF EXPERIMENTAL NOISE AND ITS INFLUENCE

First, we show that the entropy is significantly more sensitive to the purity of a quantum state under small noise compared with the state fidelity. Our experiment concerns about the entropy of a qubit system, and the purity of quantum state of a qubit can be quantified by the length of the Bloch vector for the state. The qubit state can always be represented by a Bloch sphere and the Bloch vector length L , defined as $L = |2p - 1|$, where p and $1 - p$ are the two eigenvalues of the density matrix of a single-qubit state. Apparently pure states have $p = 1$ and $L = 1$. The relation between the Bloch vector length L and the von Neumann entropy S (or the Shannon entropy in the diagonal basis) is given by

$$\begin{aligned} S &= (-p \log_2 p - (1 - p) \log_2 (1 - p)) \\ &= 1 - \frac{1}{2}[(1 + L) \log_2 (1 + L) + (1 - L) \log_2 (1 - L)]. \end{aligned} \quad (1)$$

This relation is shown in the supplementary figure 1a. First, the curve is monotonically decreasing, so the entropy always increases when the purity decreases as one expects. Second, the entropy sharply rises when the purity reduces from the maximum value 1 (as one deviates from the pure state) by the nonlinear dependence. For instance, a 10% drop in L corresponds to an increase of the entropy to 30% of its maximum value already. This is different from the state fidelity F , which is linearly dependent on the deviation $1 - L$ ($F \simeq p = 1 - (1 - L)/2$). This explains why the entropy is significantly more sensitive to noise compared with the state fidelity.

Our third experiment has the largest contribution from noise as we start from an entangled state which is more sensitive to noise including dephasing and the experimental sequence of operations is also significantly longer compared with the first two experiments. We identify two major noise contributions to the entropy increase in our system. First, the electronic spin is subject to remaining dephasing although we have implemented decoherence protected quantum gates using the dynamical decoupling pulses. At room temperature, even after correction by dynamical decoupling pulses, the coherence time for the electronic spin is still limited to be well below 1 ms. For instance, in the supplementary figure 1b, we show the detected coherence decay of the electronic spin after application of the Hahn spin echo in the between, with the effect measured by both the decay of the purity L and the increase of the single-spin entropy S . The decay of the Bloch vector length can be fit by the Gaussian decay envelop $\exp(-(\tau/T_2^*)^2)$, and this fitting gives an estimated $T_2^* \sim 378 \mu\text{s}$. The operation time of the whole experimental sequence in our third experiment, is about $190 \mu\text{s}$. If we take the above estimated T_2^* , the Bloch length vector will drop by about 23.4% after the experimental sequence. The second major noise contribution to our third experiment lies in the electronic spin dephasing during the time gap between two adjacent decoherence protected quantum gates. In our experiment, each CNOT gate is implemented with combination of two decoherence-protected Toffoli gates, and each Toffoli gate is coherence-protected by two symmetric dynamical decoupling pulses (see Fig. 4a of the main text). The experimental microwave and RF pulses for the Toffoli gates always have finite rising and falling times, so there are small time gaps between two adjacent Toffoli gates, which are outside the coherence protection by the dynamical decoupling pulses. The decoherence rate for the unprotected time window should be estimated by $1/T_2^*$, where T_2^* denotes the free-induction decay time for the electronic spin without the spin echo. The free induction decay time T_2^* depends on the external magnetic field and could range from $1.7 \mu\text{s}$ to $3.6 \mu\text{s}$ as measured in [1, 2]. For our experiment, we estimate $T_2^* \sim 2.5 \mu\text{s}$. The total time gaps t_Δ between the adjacent Toffoli gates in our whole experimental sequence adds up to about $1.2 \mu\text{s}$, and the dephasing during those unprotected gaps will contribute another 20.6% decay of the Bloch vector length through estimation by a similar Gaussian decay envelop $\exp(-(t_\Delta/T_2^*)^2)$. As a result, the estimated remaining length of the Bloch vector becomes $(1 - 0.234) \times (1 - 0.206) = 0.608$, which would correspond to an entropy of 0.72 (in contrast to the zero entropy in the ideal case). This value is close to what we observed

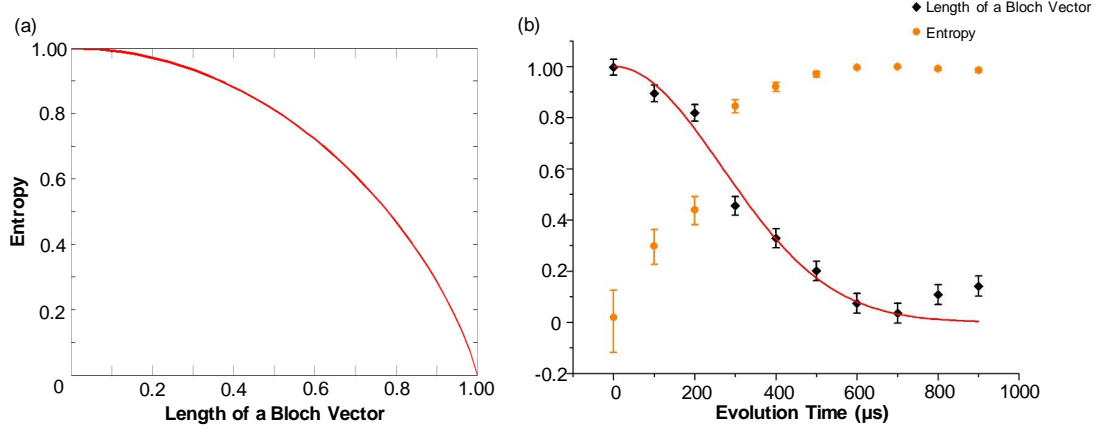


FIG. 1: **Entropy variation under experimental noise.** **a**, Variation of the entropy with the length of Bloch vector which characterizes the purity of a quantum state. It is given by a monotonic but nonlinear relation with the function $y = 1 - [(1+x)\log_2(1+x) + (1-x)\log_2(1-x)]/2$. One can see that entropy increases quickly when the Bloch vector length deviates from 1, explaining the sensitivity of entropy under small noise compared with the state fidelity. **b**, Decay of the length of Bloch vector under free evolution with a Hahn echo (dynamical decoupling) pulse applied at the middle point of the evolution. The external magnetic field is set at 340 Gauss. The data can be fit with a Gaussian envelop $\exp[-(\tau/T_2)^2]$ with $T_2 \sim 378 \mu\text{s}$.

in the third experiment as shown in Fig. 4c for the main text. For the initial state, the system should be in a maximally mixed state and have entropy $S = 1$. However, due to small imperfection in the experimental calibration and preparation, we have a measured entropy about 0.90 in our experiment (see Fig. 4c, note that this corresponds to a pretty high preparation fidelity about 98%). Combining the entropies estimated from the above analysis, we have the entropy decrease $\Delta S = 0.90 - 0.72 = 0.18$ for our third experiment, which roughly agrees with what we observed experimentally.

SUPPLEMENTARY NOTE 2: INFLUENCE OF IMPERFECT INITIAL STATE POLARIZATION

In our experiment, we have used the same method as in Refs. [3, 4] to calibrate the fluorescence counts for different spin states and to normalize our experimental results. This is a widely used calibration method in diamond NV center experiments which effectively subtracts the influence of the imperfection in the initial state polarization. To see how it works, we describe the electronic spin state with imperfect initial polarization by the density operator

$$\rho = p_0 \rho_0 + (1 - p_0) I_2/2 \quad (2)$$

where ρ_0 denotes the effective initial state (usually pure), I_2 is the 2×2 identity matrix, and p_0 denotes the polarization probability, which is typically about 84% for a diamond NV center at room temperature [5]. Any operations on the state ρ leaves the second part $I_2/2$ unchanged, and this is even true for general non-unitary operations. For the fluorescence count measurements on the diamond NV center, we calibrate the count contrast right after the state initialization and defines the underlying state as $|0\rangle$ ($|1\rangle$) when the count reaches the maximum (minimum) [3, 4]. For the final state measurement, we use this calibrated count contrast to measure the state fraction in $|0\rangle$ or $|1\rangle$ components. As the term $(1 - p_0) I_2/2$ in ρ has no influence on the count contrast, it only contributes a background noise and we effectively subtract the influence of this term from both the initial and the final states.

As we have subtracted the same identity term in the initial and the final state by this normalization method, the observation of an entropy decrease (or increase) should be independent of this background noise subtraction. Note that the second term $(1 - p_0) I_2/2$ has zero contribution to the length of the Bloch vector, and the normalization factor p_0 in the first term $p_0 \rho_0$ reduces the Bloch vector length L for the initial and the final states by the same ratio, so it will not change its direction of variation. As the entropy monotonically depends on the state purity, its decrease (or increase) does not depend on this noise subtraction, although its exact value will indeed be changed a bit. We can estimate how much entropy decreases for our system if we do not do this noise subtraction. Let us take the third experiment as an example as it has the largest contribution by noise. With the background noise subtraction, we have

observed an initial entropy about 0.88 and a final entropy about 0.76, which corresponds to an initial Bloch vector length $L_0 = 0.40$ and the final $L_f = 0.56$. Now without background noise subtraction, we should have $L'_0 = p_0 L_0$ and $L'_f = p_0 L_f$ by taking p_0 with its typical value 0.84. The corresponding entropies for the initial and the final states are given respectively by 0.92 and 0.83, so we still have an observed entropy decrease about 0.09 bit for this experiment by taking into account the contribution of the imperfect initial state polarization.

-
- [1] Zhao, Nan., Ho, Sai.-Wah. and Liu, R. B. Decoherence and dynamical decoupling control of nitrogen-vacancy center electron spins in nuclear spin baths. *Phys. Rev. B* 85, 115303. (2012)
 - [2] Childress, L., Gurudev, Dutt, M. V., Taylor, J. M., Zibrov, A. S., Jelezko, F., Wrachtrup, J., Hemmer, P. R., Lukin, M. D. Coherent dynamics of coupled electron and nuclear spin qubits in diamond. *Science* 2006, 314(5797):281. (2006)
 - [3] Dutt, M. V., Childress, L., Jiang, L., Togan, E., Maze, J., Jelezko, F., Zibrov, A. S., Hemmer, P. R., Lukin, M. D. Quantum register based on individual electronic and nuclear spin qubits in diamond. *Science* 2007, 316(5829):1312. (2007).
 - [4] Zu, C., Wang, W.-B., He, L., Zhang, W.-G., Dai, C.-Y., Wang, F. & Duan, L.-M. Experimental realization of universal geometric quantum gates with solid-state spins. *Nature* 514, 72 (2014).
 - [5] Robledo, L., Bernien, H., Sar, T. V. D., Hanson, R. Spin dynamics in the optical cycle of single nitrogen-vacancy centres in diamond. *New J. Phys.* 13, 025013. (2011)